ChemElectroChem

Research Article
doi.org/10.1002/celc.202400045

Chemistry Europe
European Chemical Societies Publishing

www.chemelectrochem.org

Low-Voltage Acidic CO_2 Reduction Enabled by a Diaphragm-Based Electrolyzer

A. Perazio,[a] Moritz W. Schreiber,[b] C. E. Creissen,*[c] and M. Fontecave*[a]

Large-scale implementation of electrochemical CO_2 conversion to value-added products is currently hampered by high electrolyzer cell voltages, resulting in low energy efficiency and high operating costs. Cell voltages are typically well above 3 V and need to be significantly lowered whilst maintaining current densities greater than 200 mA cm^{-2} to enable energy-efficient CO_2 electroreduction. This can be addressed through modification of the resistive components of the device to reduce energy consumption and lower operating costs. Electrodes, electrolyte solutions, and the separator between compartments, provide the largest contributions to the overall cell voltage, therefore decreasing their resistance can lower the electricity input required to drive effective CO_2 conversion. Here, by careful analysis and tuning of the various sources of voltage drops within the cell, an optimized diaphragm-based CO_2R device is presented, which is able to operate at an industrially relevant current density of 200 mA cm^{-2} with an $|E_{cell}|$ as low as 2.89 V, amongst the lowest reported values to date.

Introduction

Electrochemical CO_2 reduction (CO_2R) offers a sustainable pathway to convert intermittent renewable electricity into chemicals and fuels.[1] Developing a technology able to yield large amounts of valuable molecules starting from a waste product such as CO_2 would help to decouple the modern economy from fossil fuels. Industrial application of electrochemical CO_2 reduction (CO_2R) requires efficient, high-rate generation of carbon products. Critical parameters to consider for the scale-up of CO_2 electrolyzers are the current density, selectivity towards multicarbon (C_{2+}) products, CO_2 utilization, stability, and the cell voltage (E_{cell}). In previous work, the faradaic efficiency for multicarbon products (FE_{C2+}) and the CO_2 utilization have been optimized in acidic conditions.[2–6] However, the typically high cell voltages required to reach industrially-relevant current densities remain a barrier to the development of competitive CO_2 electrolysis.[7,8] Therefore, decreasing the overall E_{cell} towards the values obtained for H_2O electrolyzers has the potential to reduce operating costs and improve access to sustainable fuels.[9]

High-rate CO_2 electrolysis can be facilitated using gas-fed flow cells (GFFCs) and membrane electrode assemblies (MEAs). Due to their modularity, many studies have focused on improving the performance (in terms of selectivity, and energy efficiency, among others) by altering components (catalyst, membrane)[10–13] or conditions (temperature, pressure, pH).[14–16] A major development in recent years has been the incorporation of acidic electrolyte solutions in GFFCs that prevent permanent CO_2 loss as (bi)carbonate and can therefore boost the conversion of CO_2R products.[2–5] However, acidic conditions have so far restricted the type of membrane that can be used to either bipolar membranes (BPMs) or cation exchange membranes (CEMs), which can lead to high cell voltages.[2,3,17] While CEMs provide effective proton transport, it is preferable to keep the anolyte free from metal cations which can cross the membrane and accumulate in the catholyte, leading to an increase in pH. In addition, CEMs impart a significant resistance to the passage of positively charged species, which negatively impacts the cell voltage.[18] On the other hand, BPMs prevent crossover and enable different catholyte and anolyte pH to be used,[19] but add an important voltage penalty (at least 0.83 V at 100 mA cm^{-2}),[20] due to the process of water dissociation that occurs at the interface between the ion exchange layers.[21] An alternative solution is to use a non-ion-selective diaphragm that displays low resistance to charge crossover, greatly reducing the voltage drop at the compartment separator. Although such diaphragms are commonplace in water electrolyzers,[22,23] they have not been used for CO_2R, as the formed liquid products can diffuse to the anode where they could be potentially oxidized.

The objective of this work is to assess different approaches to significantly reduce the cell voltage of a CO_2 electrolyzers. Here, we explored how the use of a diaphragm, increased operating temperature, and optimization of the cell architecture could reduce the E_{cell}. Furthermore, external electrolyte mixing was employed to obtain a stable system for long-term electrolysis. By monitoring voltage, selectivity, and carbon mass balance, we highlight advantages of diaphragm-based devices

[a] A. Perazio, M. Fontecave
Laboratoire de Chimie des Processus Biologiques, CNRS UMR 8229, Collège de France, 75231Paris, France
E-mail: m.fontecave@college-de-france.fr

[b] M. W. Schreiber
Total Research and Technology, Refining and Chemicals, Division CO2 Conversion, Feluy, 7181 Seneffe, Belgium

[c] C. E. Creissen
School of Chemical and Physical Sciences, Keele University, Staffordshire, ST5 5BG, UK
E-mail: c.e.creissen@keele.ac.uk

Supporting information for this article is available on the WWW under https://doi.org/10.1002/celc.202400045

and present a future direction for low-voltage CO_2 electroreduction.

Cell Configuration and Voltage Contributions

All systems studied here were based on previously reported GFFC configurations composed of a cathode chamber and an anode chamber divided by a physical separator (Figure 1).[2,19,24,25] In this configuration, the CO_2 is supplied through a gas channel and passes through the gas diffusion electrode to react at the catalyst/catholyte interface. As the catalyst is directly deposited on a hydrophobic gas diffusion layer (PTFE), liquid is prevented from crossing into the gas channel. A gas-diffusion cathode composed of Cu nanoparticles on a PTFE support was used, with the cathode directly contacted with the gas-flow plate for all systems. Additionally, an IrO_x layer deposited on porous carbon paper was used as the anode. However, as other components and distances will be varied, we have used a notation for the configurations: $||$ **C** $|$ $\mathbf{d_{cs}}$ $|$ **S** $|$ $\mathbf{d_{as}}$ $|$ **A** $|$ $\mathbf{d_{ab}}$ $||$, in which **II** are the endplates, **C** is the cathode, $\mathbf{d_{cs}}$ is the cathode-separator distance, **S** is the separator type, $\mathbf{d_{as}}$ is the anode-separator distance, **A** is the anode, and $\mathbf{d_{ab}}$ is the anode backplate separation. All **d** values are given in mm.

The full cell voltage of a gas-fed flow cell is composed of voltage contributions from the cathode reaction (E_{red}), the anode reaction (E_{ox}), the voltage drops (E_{loss}) associated with the resistance of the separator (E_{sep}), the resistance of the solution and ionic diffusion gradients (E_{sol}), and the pH difference between the cell compartments (E_{pH}, $\Delta pH = pH_{catholyte} - pH_{anolyte}$). In Equations 1–5 the modulus for E_{cell}, E_{loss}, E_{red}, and E_{ox} was used to obtain absolute values.

$$|E_{cell}| = |E_{red}| + |E_{ox}| + |E_{loss}| \quad (1)$$

$$E_{red} = E^{o}_{red} - \frac{RT}{nF}\ln(Q) + \eta_{red} \quad (2)$$

$$E_{ox} = E^{o}_{ox} - \frac{RT}{nF}\ln(Q) + \eta_{ox} \quad (3)$$

$$E_{loss} = |E_{sol}| + |E_{sep}| + E_{pH} \quad (4)$$

$$E_{pH} = \frac{2.303\ RT}{F}\Delta pH \quad (5)$$

The E_{red} and E_{ox} terms are dictated by the thermodynamics of the products formed at the electrodes and their relative overpotentials (η) for a given catalyst. As the same electrodes and catalysts were used throughout the work, the only modifications to these values are due to changes in temperature and pH, which are linked to the half-cell potential through the Nernst equation (Equations 2 and 3, where n is the number of electrons, R is the universal gas constant, T is the temperature, F is the Faraday constant, and Q is the reaction quotient). The focus of this study concerns specific contributions to the E_{loss} term, which will be evaluated by assessing the voltage penalties related to the electrolyte solution and the separator (i.e. E_{sol}, E_{sep}).

The conductivity of an electrolyte solution and the resulting solution resistance is defined by the nature of the salts, the distance through which the ions must be transported, the concentration of each species, and the conditions of the system (e.g. temperature, pressure).[26] Here, we consider three key parameters: the electrolyte solution composition, the distance between the electrodes, and the temperature of the electrolyte

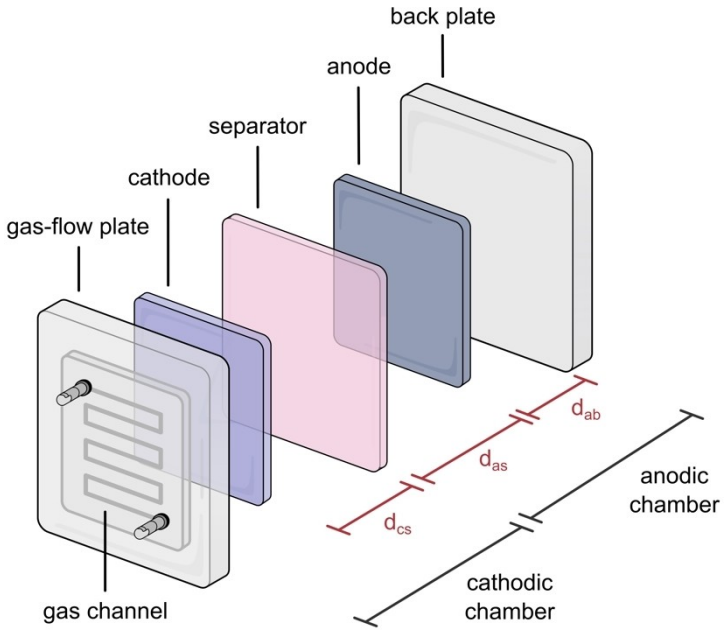

Figure 1. Illustration of the main elements of a gas-fed flow cell. d_{cs}: distance between cathode and separator; d_{as}: distance between anode and separator; d_{ab}: distance between anode and back plate. The separator can either be a cation-exchange membrane or a diaphragm.

solution. As for the separator, a cation ion exchange membrane is typically used to prevent gas, anion, and liquid product crossover. However, this introduces a significant resistance and increases E_{sep}, which is dependent on the type of membrane used and also on the reaction conditions (electrolyte composition and pH).[12] We therefore investigated the use of a diaphragm separator as a novel approach to reduce the E_{sep} contribution. However, to compare the performance to a standard setup, we first used a CEM-based electrolyzer for subsequent alterations.

CEM-Based Electrolyzer

GFFCs for acidic CO_2R typically employ a cation exchange membrane (CEM), an acidic catholyte containing alkali metal cations (typically K^+ or Cs^+) and an acidic anolyte.[27–29] Therefore, we initially designed a CEM system as a starting point for modification.

Initially, a standard catholyte containing 3 M KCl and 0.05 M H_2SO_4 (pH 1) was used with a Nafion 115 CEM and a 1 M H_2SO_4 anolyte (pH 0.4) – this configuration was denoted | | **C** | **4** | **CEM** | **4** | **A** | **0** | | (an illustration of the full GFFC setup is shown in Figure S1). The measured $|E_{cell}|$ was 3.61 V for a current density of 200 mA cm^{-2}, while the product selectivity showed that CO production was favored over C_2H_4, alongside minor H_2 formation as previously observed for this setup (Figure S2).[2] The high voltage required to reach 200 mA cm^{-2} can be partly attributed to the CEM component, which facilitates the transport of cations through electrostatic interactions with the negatively charged functional groups within their structures (sulfonic acid groups in the case of Nafion), giving rise to resistance.[30] The membrane resistance depends on the nature of the cation,[18] and therefore its contribution to the cell voltage (E_{sep}) plays a large role when the typically high salt concentrations required to prevent H_2 evolution are used in acidic CO_2R.

An additional drawback of this setup is that the choice of the anolyte is restricted to metal-cation-free solutions. This is because metal cations can migrate from the anode compartment towards the cathode compartment in competition with protons that are present in solution already, or that are generated by the anodic reaction. The preferential cation transport leads to an increased pH in the catholyte over time since the protons consumed by CO_2R are not replenished.[31] The cation transport is unidirectional and driven by the internal electric field in the cell, and therefore is only problematic for anolyte cations rather than catholyte cations with a CEM-based system. We showed this experimentally by performing electrolysis with two separate systems, for which the anolyte contained K^+ (Figure S3a) or no cationic species (Figure S3b). With 1 M K_2SO_4 present in the anolyte, preferential K^+ transport resulted in an increased pH at the cathode (Figure S3a), however when only H^+ was present, the protons depleted at the cathode were continuously replenished by those coming from the anolyte, and the pH was constant over several hours (Figure S3b).

Due to the issues introduced by the utilization of a CEM, an alternative compartment separator was assessed to reduce the associated voltage drop.

Diaphragm-Based Electrolyzer

We aimed to replace the CEM with a diaphragm to reduce the resistance and E_{sep}. For this, we employed Zirfon, a well-known separator used for alkaline water electrolysis applications, consisting of a hydrophilic composite diaphragm comprising a polysulfone matrix and a zirconium oxide inorganic filler.[23,32–34] With no charged groups, Zirfon is a non-ion-selective separator and its conductivity is only determined by the electrolyte used;[35] hence, the diaphragm imparts less resistance to charge transport compared with Nafion. To compare the charge transport resistance of Zirfon and Nafion, the voltage drop of the separator in contact with the electrolyte ($|E_{sep}|$) was measured, as the voltage drop depends on the working conditions and therefore reflects the total contribution of the separator to the E_{cell}. When tested in the same conditions, the $|E_{sep}|$ for a Zirfon-based system (0.26 V) was lower than that of an identical Nafion setup (0.93 V) (Figure 2). The lack of selectivity allows any solution-phase species, either charged or neutral, to cross from one side of the cell to the other, while gas crossover is prevented. This makes the diaphragm suitable for a system using the same electrolyte in both cell compartments.

Electrolyte Selection

Selecting the most appropriate ions for low resistance solutions is not straightforward due to the wide range of possible salts, but molar ionic conductivity values can be used to guide the electrolyte selection to provide highly conductive solutions (Figure S4).[36,37] The previously described CEM system used 3 M KCl, which is highly soluble (340 g L^{-1}, 20 °C), but does not exhibit high ionic conductivity values (K^+: 73.5 S cm^2 mol^{-1}, Cl^-: 76.3 S cm^2 mol^{-1}). As 3 M KCl is a concentration close to the saturation point, the salt content cannot be increased to improve the conductivity. Furthermore, Cl^- can be oxidized at the anode to generate toxic Cl_2 gas. A non-chloride-based salt able to provide a higher ionic strength would therefore increase the solution conductivity and help improve the E_{cell}.

Alkali cations are essential to favor CO_2R over HER in acidic solutions, with weakly hydrated ions being more effective due to their stronger propension to adsorb on the negatively charged cathode ($Li^+ < Na^+ < K^+ < Cs^+$).[3,38,39] We tested a number of potassium salts, however these showed limited success due to either their low solubility or excessive H_2 production (Figure S5). We therefore turned our attention to Cs_2SO_4, as the larger cations display weaker hydration and possess a remarkably high solubility (1790 g L^{-1}, 20 °C), providing ions with a good ionic conductivity (77. 3 S cm^2 mol^{-1} for Cs^+ and 160.0 S cm^2 mol^{-1} for SO_4^{2-}). With 1.5 M and 3 M Cs_2SO_4, the E_{red} values were −1.2 V and −1.1 V respectively, demonstrating the high conductivity of the electrolyte solution

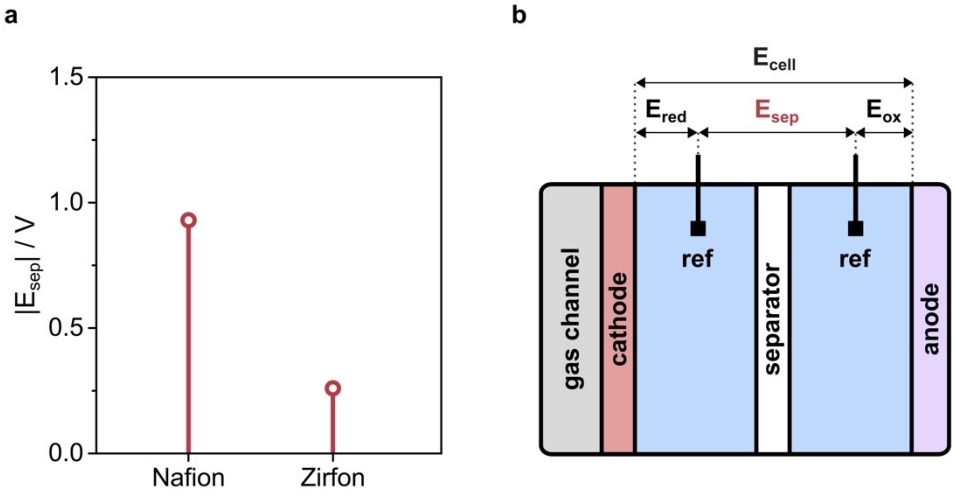

Figure 2. (a) Comparison of $|E_{sep}|$ between two identical setup featuring either Nafion or Zirfon as a separator. (b) Illustration of the cell setup. E_{sep}, E_{red} and E_{ox} also account for part of the solution voltage drop, E_{sol}. In this test, E_{red}, E_{ox}, and E_{sol} are constant, therefore the variation if E_{sep} is due to the different compartment separator. Conditions: 3 M KCl/0.05 M H_2SO_4 catholyte (pH 1), 3 M KCl/0.05 M H_2SO_4 anolyte (pH 1), 20 mL min^{-1} feed CO_2 flow rate, -200 mA cm^{-2}, | | **C** | **4** | **separator** | **4** | **A** | **0** | | configuration.

(Figure S5e), and CO_2R was favored over HER. Cs_2SO_4 was therefore chosen as an appropriate salt to evaluate the performance of the diaphragm-based electrolyzer.

One-Gap Diaphragm Electrolyzer

In a | | **C** | **4** | **DIA** | **4** | **A** | **0** | | configuration with 1.5 M Cs_2SO_4 (pH 5, adjusted through addition of H_2SO_4), the $|E_{cell}|$ value was 3.90 V for an applied current density of 200 mA cm^{-2}. However, upon increasing the salt concentration to 3 M Cs_2SO_4 (pH 5), the $|E_{cell}|$ was reduced to 3.67 V (Figure 3a). At this stage, the global product distribution is not a concern and the selectivity of gas products was measured only to verify that CO_2R remained predominant over hydrogen production.

The distance between the cathode and the anode influences the overall $|E_{cell}|$, since a larger distance results in thicker layers of electrolyte between the electrodes and therefore higher $|E_{sol}|$. The | | **C** | **4** | **DIA** | **4** | **A** | **0** | | system can be described as a two-gap reactor, as there are two gaps filled with electrolyte separating the electrodes, with the diaphragm in between. By removing the gap between the diaphragm and the anode, a one-gap reactor setup can be obtained. We did so by placing the anode in direct contact with the Zirfon, while the cathodic side was unchanged, as required for acidic CO_2R. As the anode is composed of IrO_x deposited on porous carbon paper, the anolyte can flow between the electrode and the backplate, thereby maintaining the contact between the electrolyte solution and the anode catalyst. This one-gap configuration is denoted as | | **C** | **4** | **DIA** | **A** | **4** | | with the

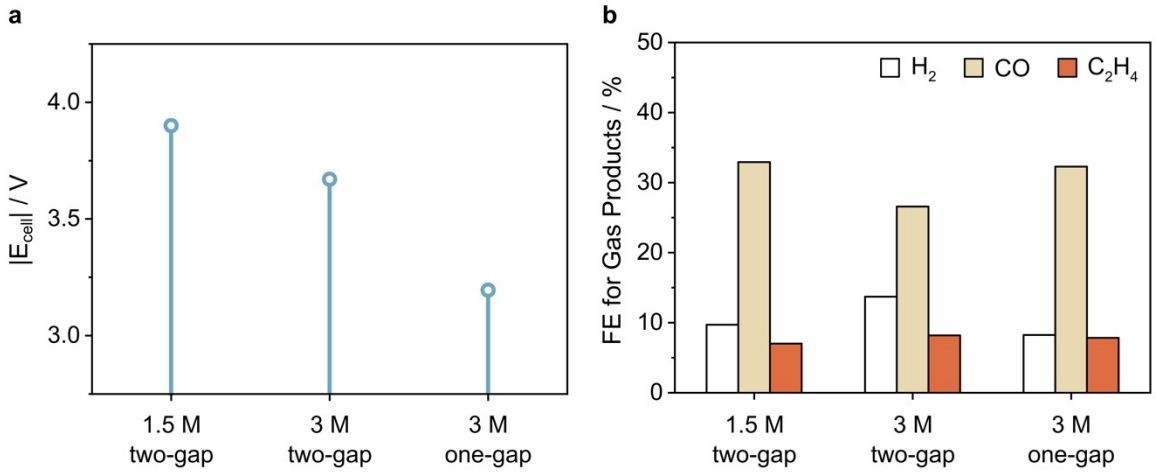

Figure 3. (a) |Ecell| optimization with the electrolyzer in a | | **C** | **4** | **DIA** | **4** | **A** | **0** | | (two-gap) and a | | **C** | **4** | **DIA** | **A** | **4** | | (one-gap) configuration and (b) corresponding gas product Faradaic efficiency (FE), with different Cs_2SO_4 concentrations (both solutions have a pH around 5) and cell configuration. Electrolysis was carried out for 30 min each at 200 mA cm^{-2} with an inlet flow rate of CO_2 of 20 mL min^{-1}.

electrodes separated by a distance of 4.5 mm. In this arrangement with 3 M Cs_2SO_4, the $|E_{cell}|$ dropped to 3.20 V, whilst maintaining the same gas product distribution (Figure 3).

The one-gap diaphragm-based system with Cs_2SO_4 afforded an E_{cell} value 0.41 V lower than that obtained for the two-gap CEM-based electrolyzer. However, similarly to the Nafion system shown in Figure S3a, the electromigration of Cs^+ from the anode to cathode resulted in an increased catholyte pH due to preferential cation crossover as opposed to protons. As a result, after 30 min of electrolysis with this one-gap diaphragm-based electrolyzer, the catholyte pH increased from pH 5 to 11, while the anolyte pH decreased to pH 2. We therefore explored the possibility of developing an externally mixed electrolyte solution setup to maintain solution pH and composition constant during electrolysis.

Electrolyte Solution Mixing Stabilizes Operation

In commercial water electrolysis, the catholyte and anolyte solutions can be mixed externally to account for any differences in time-dependent pH or concentration fluctuations so that they are eventually balanced. Mixed electrolyte solutions have also been used to equilibrate the electrolyte composition during CO_2 electrolysis to CO with silver GDEs,[40–42] however there are no previous reports investigating the effects of the mixing in complex systems where several gaseous and liquid CO_2R products are formed.

Implementing a mixed electrolyte setup with the one-gap Zirfon-based electrolyzer required some additional components to facilitate effective mixing and to avoid parasitic losses. The electrolyte was injected into both cell compartments from a main reservoir using peristaltic pumps (Figure 4). The solution coming from the cathode chamber (rich in CO_2R products, CO_2 and H_2) was directly recollected in the main reservoir (catholyte outlet **3**), while the liquid output of the anodic compartment (anolyte outlet **4**) required degassing in a separate reservoir (degassing reservoir) to remove the anodically-generated oxygen before being transferred to the main reservoir with a second pump (degassing reservoir liquid outlet **5**). In the absence of this degassing setup, O_2 can be reduced at the cathode, competing with CO_2 for the available electrons. No oxygen could be detected in the headspace of the main reservoir following degassing of the anolyte liquid output, confirming that O_2 was prevented from reaching the cathode. Gas reduction products and unreacted CO_2 were collected in the gas trap through the direct outlet of the cell (**7**) and the gas outlet of the main reservoir (**8**), and were detected using online gas chromatography (gas trap outlet **9**), while liquid products were quantified by ^{1}H NMR. Gas flow rates were monitored using multiple flow meters and a full carbon mass balance was ensured (see below). As shown in Figure S6, we verified that mixing the electrolyte had no effect on the $|E_{cell}|$ and product selectivity over 30 min electrolysis, and that the pH at each side of the reactor remained constant over the course of 3 h electrolysis. Therefore, the mixed diaphragm-based electrolyzer enhanced electrolyte stability without affecting the performance. It is worth noting that implementing a mixed 3 M Cs_2SO_4 electrolyte with a Nafion membrane (| | **C** | **4** | **CEM** | **4** | **A** | **0** | |) resulted in an $|E_{cell}|$ of around 9 V, highlighting the incompatibility of Nafion with cesium sulfate, which may stem from the strong interaction between Cs^+ ions and the sulfonic groups of Nafion.[43]

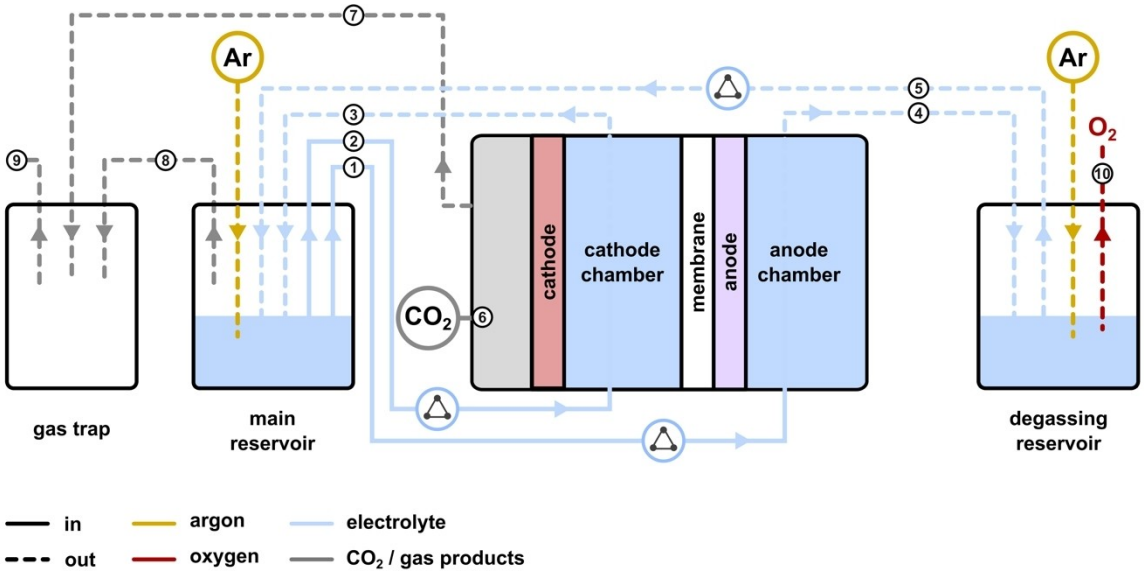

Figure 4. Illustration of the mixing setup with the | | **C** | **4** | **DIA** | **A** | **4** | | configuration. (1) catholyte inlet, (2) anolyte inlet, (3) catholyte outlet, (4) anolyte outlet, (5) degassing reservoir liquid outlet, (6) CO_2 inlet, (7) direct outlet, (8) main reservoir outlet, (9) gas trap outlet to GC, (10) degassing reservoir gas outlet.

Assessing the Degree of Liquid Product Oxidation

Even though electrolyte mixing did not seem to affect the product distribution, liquid CO_2R products building up in solution over time would likely reach the anode and be oxidized. Therefore, the propensity for oxidation of such products was assessed in the mixing setup. We evaluated the oxidation properties of the three major liquid products: formic acid, ethanol, and propanol. Water electrolysis was conducted (HER at the cathode and OER at the anode) before adding one of the products to the electrolyte solution. The amount of the products added roughly represents the amount of the same species formed during a 30 min electrolysis at 200 mA cm^{-2}.

In the first test, ethanol was added to a 3 M Cs_2SO_4 solution (pH 5) after 5 minutes of water electrolysis to obtain a concentration of 1.4 mM. Ethanol was gradually transformed into acetic acid, with near complete consumption after 160 minutes (Figure 5a). At the end of the electrolysis, the total amount of carbon species (residual ethanol + accumulated acetate/acetic acid) accounted for 93% of the ethanol added at the beginning, the remainder being attributed to overoxidation to CO_2, as verified using GC analysis and considering that a molecule of ethanol would be ultimately oxidized to two molecules of CO_2. Propanol oxidation to propionic acid behaved similarly (Figure 5b). In this case the carboxylic acid accumulated in solution more slowly and the total amount of the two species decreased progressively over time. After 120 min, only 54% (residual propanol + accumulated propionic acid) of the initial propanol amount (1.2 mM) was left. The CO_2 molar flow recorded during the test corresponds well with the missing 46%, considering that propanol complete oxidation gives 3 molecules of CO_2 per molecule of alcohol. Formic acid oxidation to CO_2 was more straightforward as there are no intermediate products (Figure 5c), and after 190 min it was completely oxidized (initial concentration: 2.8 mM). We additionally checked the ability of blank carbon paper (the anode support) to be oxidized into CO_2, but observed no significant CO_2 evolution during electrolysis, verifying that liquid product oxidation was responsible.

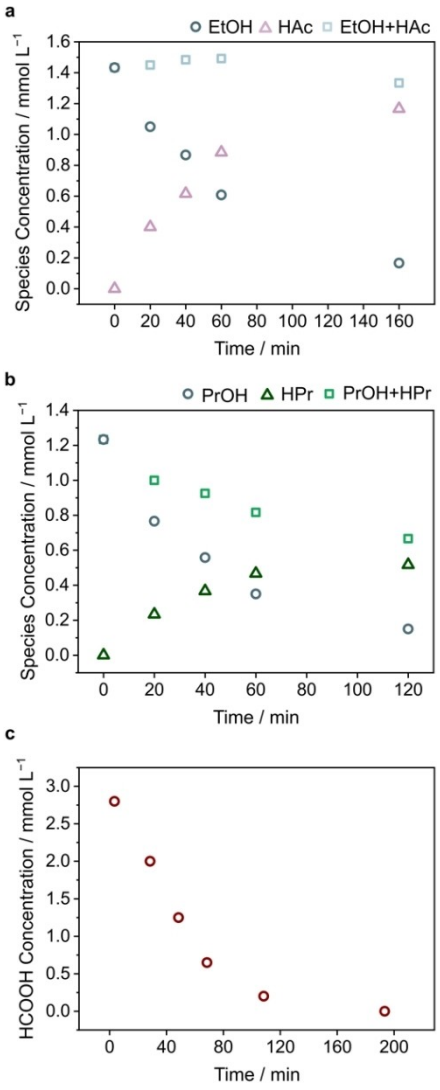

Figure 5. Results of the three oxidation tests: (a) ethanol; (b) propanol; (c) formic acid. Electrolysis was carried out in a mixing | | **C** | **4** | **DIA** | **A** | **4** | | configuration at 200 mA cm^{-2} with no flowing CO_2 and a 3 M Cs_2SO_4 electrolyte (pH 5, 20 mL).

The assessment of anodic oxidation evidenced that care must be taken when dealing with a mixing setup involving CO_2R liquid products, and that their oxidation can possibly lead to a decreased total FE if the products are lost as CO_2. Nevertheless, if the overoxidation to CO_2 can be limited, oxidation products such as carboxylic acids might be of interest.[44] It is worth noting that the selectivity shown in Figure S6 for the mixing system does not reflect liquid product oxidation. This is probably due to different reaction kinetics since in this case the amount of species in solution starts from zero and their concentration during the 30 min electrolysis reflects continuous production at the cathode and oxidation at the anode. Finally, this issue can potentially be avoided by implementing a catalyst selective towards gas products such as CO and C_2H_4.

The carbon mass balance of the reactor was evaluated to ensure that no CO_2 losses occurred in the mixing setup. Overall, mass balance was maintained even with the mixing electrolyte (Figure S7), confirming the absence of unwanted reactant losses. A detailed description is provided in the Supporting Information.

Increasing Temperature Reduces the Cell Potential

Industrial electrolyzers operate at high temperatures that originate from resistive losses. Higher working temperatures could reduce the cell voltage by decreasing the potentials and voltage drops associated with kinetic and thermodynamic contributions of CO_2 reduction.[45] There are several reported examples that investigate the temperature effects on the performance of CO_2R systems.[13,45–52] However, most of these reports focus mainly on formic acid and carbon monoxide, while neglecting systems forming multicarbon products, or do not conduct analysis in flow cells. Here, we assessed the impact of elevated electrolyte solution temperatures in our system.

Although this temperature varies inside the cell due to the addition of gas and limited insulation, the electrolyte solution temperature is quite consistent and gives a good measure of the ways in which cell voltage can be further improved.

When the temperature of the electrolyte was increased from 20 °C (room temperature) to 60 °C, the $|E_{cell}|$ was reduced from 3.2 V to a remarkable value of 2.89 V for a current density of 200 mA cm^{-2}, representing a further overall gain of 0.31 V (Figure 6a). The decrease in $|E_{cell}|$ did not come at the expense of the selectivity and a comparable product distribution was maintained from 20 °C to 60 °C (Figure 6b). With the increase in temperature, lower $|E_{red}|$, $|E_{ox}|$, and $|E_{sol}|$ values contributed to the decrease in $|E_{cell}|$.

Increasing the CO_2 Conversion Results in High Multicarbon Product Selectivity

As shown above, the system described here yields mostly C_1 products (CO and HCOOH). Steering the selectivity towards C_{2+} species is possible through decreased feed CO_2 flow rate, as previously shown by our group.[2] Lowering the flow rate from 20 mL min^{-1} to 1.25 mL min^{-1} increased the cell voltage ($|E_{cell}| = 3.17$ V at 60 °C) (Figure 7a), and simultaneously boosted the selectivity for multicarbon products at the expense of C_1 products (Figure 7b). At low flow rates, CO has a longer residence time in the reactor and therefore has more time to react on the catalyst surface to give multicarbon products, resulting in a higher amount of ethylene and ethanol. As we maintain the same current density, this results in a greater portion of the inlet CO_2 being consumed at low flow rates,

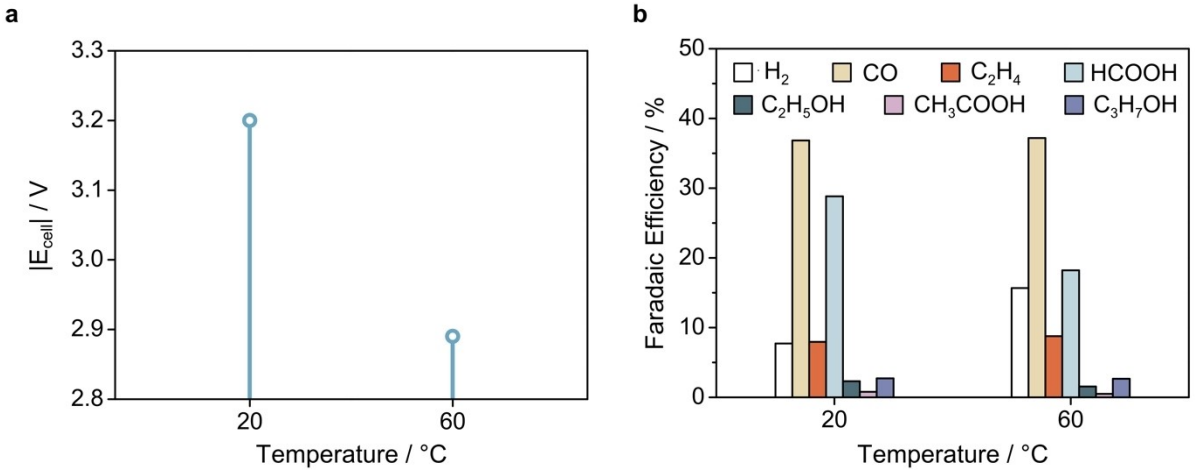

Figure 6. Effects of the electrolyte solution temperature. (a) Cell voltage decrease due to the increase in temperature and (b) relative product distribution for the three tests. Electrolysis was carried out for 30 min each at 200 mA cm^{-2} with a feed flow of CO_2 of 20 mL min^{-1} in a 3 M Cs_2SO_4 solution (pH 5) and a mixing | | **C** | **4** | **DIA** | **A** | **4** | | configuration.

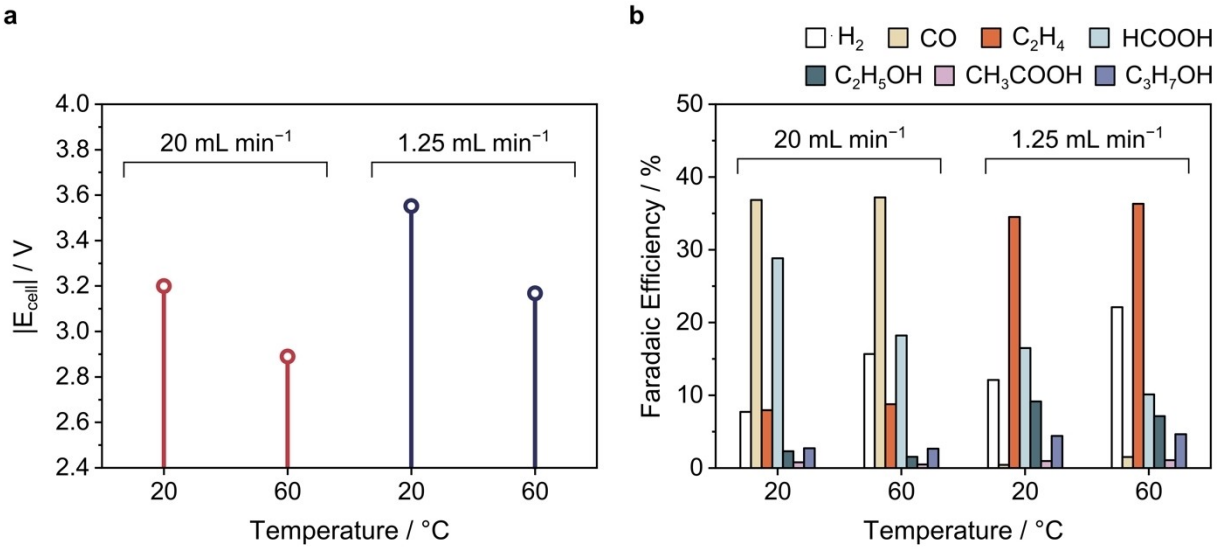

Figure 7. CO_2 feed low rate and temperature influence on cell voltage (a) and product selectivity (b). Electrolysis was carried out for 30 min each at 200 mA cm^{-2} in a 3 M Cs_2SO_4 solution (pH 5) and a mixing | | **C** | **4** | **DIA** | **A** | **4** | | configuration.

improving the likelihood of CO reduction. As this reaction typically requires larger overpotentials, we hypothesize that this enhancement in CO reduction rate is responsible for the increased cell voltage, however further work is required to verify this which is beyond the scope of the current study. The FE for CO decreased from 37% to 2%, while C_2H_4 was particularly affected with the FE increasing from 9% to 36%. FE values for C_2H_5OH and C_3H_7OH also increased, while HCOOH production diminished. The single-pass conversion efficiency for carbon products achieved for the low-flow operation was 33%. The product distribution is not affected by electrolyte mixing and temperature variation (Figure S8). Therefore, by adjusting the CO_2 flow rate, the product output of the device can be tailored to target high added-value C_{2+} products like C_2H_4.

Voltage Optimization Summary

The voltage optimization for the Zirfon-based system is summarized in Figure 8a–b. The cell potential could be lowered from 3.90 V to 2.89 V, a gain of more than 1 V. The main contributions for the optimization were: (i) increased cesium sulfate concentrations (from 1.5 M to 3 M, both pH 5), which reduced the $|E_{cell}|$ by 0.23 V; (ii) decreased electrode spacing (from 8.5 mm to 4.5 mm, with 3 M Cs_2SO_4), resulting in a gain of 0.47 V; (iii) higher temperature (from 20 °C to 60 °C, with 3 M Cs_2SO_4 and 4.5 mm electrodes distance), which lowered the cell voltage by 0.31 V. The mixing did not affect the voltage, but it stabilized the electrolyte over time in terms of pH and species concentration. It is important to note that when applying the same modifications to the initial || **C** | **4** | **CEM** | **4** | **A** | **0** || setup ($|E_{cell}| = 3.61$ V), thereby obtaining a || **C** | **4** | **CEM** | **A** | **4** || configuration, the voltage could not be lowered to the same extent and gave an $|E_{cell}|$ value of 3.24 V at 60 °C (Figure 8c–d). It is therefore evident that the resistance introduced by Nafion is a significant barrier to lowering the cell voltage, which can be overcome by employing a diaphragm.

Conclusions

The work presented here highlights a combination of strategies to lower the cell voltage of an acidic CO_2 electrolyzer by tackling its resistive components. By replacing a commonly used CEM with a diaphragm, minimizing the inter-electrode distance, and increasing the temperature to 60 °C, the cell voltage required to reach a current density of 200 mA cm^{-2} was reduced from 3.61 V to 2.89 V, a value approaching that needed for scale-up and commercialization. Through assessment of the contributing potentials and products, we showed that the setup could operate with good selectivity and activity with a mixed

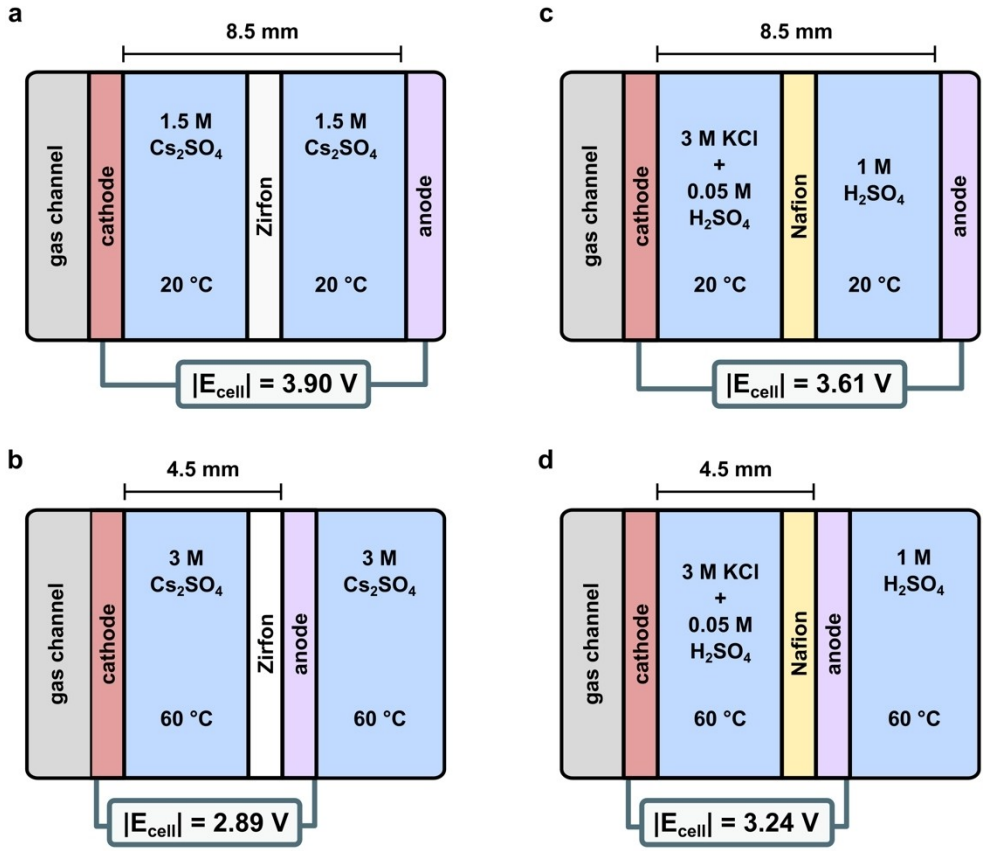

Figure 8. Optimization summary for the Zirfon- (a, b) and the Nafion- (c, d) based systems at 200 mA cm^{-2}. (a) || **C** | **4** | **DIA** | **4** | **A** | **0** ||; (b) || **C** | **4** | **DIA** | **A** | **4** ||; (c) || **C** | **4** | **CEM** | **4** | **A** | **0** ||; and (d) || **C** | **4** | **CEM** | **A** | **4** ||.

electrolyte solution. By ensuring a full carbon mass balance, we showed that although some liquid products were oxidized in this setup, there was limited overoxidation of high-value C_{2+} products to CO_2 and therefore such setups could be practicable for generation of carboxylic acids.

We envisage that modifications including implementing catalysts that require lower half-cell potentials and further reduction of the inter-electrode distance will benefit the cell potential. Overall, the outcomes of this study are fundamental to building robust and efficient systems that can propel CO_2 electrolysis towards commercialization.

Conflict of Interests

The authors declare no conflict of interest.

Data Availability Statement

The data that support the findings of this study are available from the corresponding author upon reasonable request.

[1] D. Karapinar, C. E. Creissen, J. G. Rivera De La Cruz, M. W. Schreiber, M. Fontecave, *ACS Energy Lett.* **2021**, *6*, 694–706.
[2] A. Perazio, C. E. Creissen, J. G. Rivera de la Cruz, M. W. Schreiber, M. Fontecave, *ACS Energy Lett.* **2023**, *8*, 2979–2985.
[3] J. E. Huang, F. Li, A. Ozden, A. S. Rasouli, F. P. G. de Arquer, S. Liu, S. Zhang, M. Luo, X. Wang, Y. Lum, Y. Xu, K. Bertens, R. K. Miao, C. T. Dinh, D. Sinton, E. H. Sargent, *Science* **2021**, *372*, 1074–1078.
[4] J. Gu, S. Liu, W. Ni, W. Ren, S. Haussener, X. Hu, *Nature Catalysis* **2022**, *5*, 268–276.
[5] Y. Xie, P. Ou, X. Wang, Z. Xu, Y. C. Li, Z. Wang, J. E. Huang, J. Wicks, C. McCallum, N. Wang, Y. Wang, T. Chen, B. T. W. Lo, D. Sinton, J. C. Yu, Y. Wang, E. H. Sargent, *Nature Catalysis* **2022**, *5*, 564–570.
[6] L. P. Chi, Z. Z. Niu, Y. C. Zhang, X. L. Zhang, J. Liao, Z. Z. Wu, P. C. Yu, M. H. Fan, K. Bin Tang, M. R. Gao, *Proc. Natl. Acad. Sci. USA* **2023**, *120*, e2312876120.
[7] S. S. Bhargava, D. Azmoodeh, X. Chen, E. R. Cofell, A. M. Esposito, S. Verma, A. A. Gewirth, P. J. A. Kenis, *ACS Energy Lett.* **2021**, *6*, 2427–2433.
[8] D. V. Esposito, *Joule* **2017**, *1*, 651–658.
[9] M. W. Schreiber, *Curr. Opin. Electrochem.* **2023**, *44*, 101438.
[10] D. Sun, X. Xu, Y. Qin, S. P. Jiang, Z. Shao, *ChemSusChem* **2020**, *13*, 39–58.
[11] S. Nitopi, E. Bertheussen, S. B. Scott, X. Liu, A. K. Engstfeld, S. Horch, B. Seger, I. E. L. Stephens, K. Chan, C. Hahn, J. K. Nørskov, T. F. Jaramillo, I. Chorkendorff, *Chem. Rev.* **2019**, *119*, 7610–7672.
[12] F. Habibzadeh, P. Mardle, N. Zhao, H. D. Riley, D. A. Salvatore, C. P. Berlinguette, S. Holdcroft, Z. Shi, *Electrochem. Energy Rev.* **2023**, *6*, 1–35.
[13] L. S. Cousins, C. E. Creissen, *Nanoscale* **2024**, *16*, 3915–3925.
[14] R. E. Vos, K. E. Kolmeijer, T. S. Jacobs, W. Van Der Stam, B. M. Weckhuysen, M. T. M. Koper, *ACS Catal.* **2023**, *13*, 8080–8091.
[15] L. Huang, G. Gao, C. Yang, X. Y. Li, R. K. Miao, Y. Xue, K. Xie, P. Ou, C. T. Yavuz, Y. Han, G. Magnotti, D. Sinton, E. H. Sargent, X. Lu, *Nat. Commun.* **2023**, *14*, 1–11.
[16] K. J. P. Schouten, E. Pérez Gallent, M. T. M. Koper, *J. Electroanal. Chem.* **2014**, *716*, 53–57.
[17] B. Siritanaratkul, M. Forster, F. Greenwell, P. K. Sharma, E. H. Yu, A. J. Cowan, *J. Am. Chem. Soc.* **2022**, *144*, 7551–7556.
[18] K. M. Vetter, J. Härtl, D. Reinisch, T. Reichbauer, N. Martić, K. O. Hinrichsen, G. Schmid, *ChemElectroChem* **2022**, *9*, e202101165.
[19] A. Peugeot, C. E. Creissen, M. W. Schreiber, M. Fontecave, *ChemElectroChem* **2021**, *8*, 2726–2736.
[20] R. Simons, *J. Membr. Sci.* **1993**, *78*, 13–23.
[21] R. Pärnamäe, S. Mareev, V. Nikonenko, S. Melnikov, N. Sheldeshov, V. Zabolotskii, H. V. M. Hamelers, M. Tedesco, *J. Membr. Sci.* **2021**, *617*, 118538.
[22] A. Hodges, A. L. Hoang, G. Tsekouras, K. Wagner, C. Y. Lee, G. F. Swiegers, G. G. Wallace, *Nat. Commun.* **2022**, *13*, 1–11.
[23] M. Schalenbach, W. Lueke, D. Stolten, *J. Electrochem. Soc.* **2016**, *163*, F1480–F1488.
[24] C. E. Creissen, J. G. Rivera de la Cruz, D. Karapinar, D. Taverna, M. W. Schreiber, M. Fontecave, *Angew. Chem. Int. Ed.* **2022**, *61*, e202206279.
[25] E. Vichou, A. Perazio, Y. Adjez, M. Gomez-Mingot, M. W. Schreiber, C. M. Sánchez-Sánchez, M. Fontecave, *Chem. Mater.* **2023**, *35*, 7060–7068.
[26] W. Zheng, *ACS Energy Lett.* **2023**, *8*, 1952–1958.
[27] J. E. Huang, F. Li, A. Ozden, A. S. Rasouli, F. P. G. de Arquer, S. Liu, S. Zhang, M. Luo, X. Wang, Y. Lum, Y. Xu, K. Bertens, R. K. Miao, C. T. Dinh, D. Sinton, E. H. Sargent, *Science* **2021**, *372*, 1074–1078.
[28] Y. Xie, P. Ou, X. Wang, Z. Xu, Y. C. Li, Z. Wang, J. E. Huang, J. Wicks, C. McCallum, N. Wang, Y. Wang, T. Chen, B. T. W. Lo, D. Sinton, J. C. Yu, Y. Wang, E. H. Sargent, *Nature Catalysis* **2022**, *5*, 564–570.
[29] J. Gu, S. Liu, W. Ni, W. Ren, S. Haussener, X. Hu, *Nature Catalysis* **2022**, *5*, 268–276.
[30] K. A. Mauritz, R. B. Moore, *Chem. Rev.* **2004**, *104*, 4535–4585.
[31] J. B. Vennekötter, T. Scheuermann, R. Sengpiel, M. Wessling, *J. CO2 Util.* **2019**, *32*, 202–213.
[32] P. Vermeiren, W. Adriansens, J. P. Moreels, R. Leysen, *Int. J. Hydrogen Energy* **1998**, *23*, 321–324.
[33] M. J. Lavorante, C. Y. Reynoso, J. I. Franco, *New pub: Balaban* **2014**, *56*, 3647–3653.
[34] P. Vermeiren, J. P. Moreels, R. Leysen, *J. Porous Mater.* **1996**, *3*, 33–40.
[35] M. T. de Groot, A. W. Vreman, *Electrochim. Acta* **2021**, *369*, 137684.
[36] C. Zhong, Y. Deng, W. Hu, J. Qiao, L. Zhang, J. Zhang, *Chem. Soc. Rev.* **2015**, *44*, 7484–7539.
[37] P. Abba, J. Gongwala, S. Laminsi, J. L. Brisset, *Int. J. Res. Chem. Environ.* **2014**, *4*, 25–30.
[38] J. Gu, S. Liu, W. Ni, W. Ren, S. Haussener, X. Hu, *Nature Catalysis* **2022**, *5*, 268–276.
[39] M. R. Thorson, K. I. Siil, P. J. A. Kenis, *J. Electrochem. Soc.* **2013**, *160*, F69–F74.
[40] T. Haas, R. Krause, R. Weber, M. Demler, G. Schmid, *Nature Catalysis* **2018**, *1*, 32–39.
[41] D. Reinisch, D. Reinisch, B. Schmid, N. Martić, N. Martić, R. Krause, H. Landes, M. Hanebuth, K. J. J. Mayrhofer, K. J. J. Mayrhofer, G. Schmid, *Zeitschrift Fur Physikalische Chemie-Frankfurt* **2020**, *234*, 1115–1131.
[42] R. Krause, D. Reinisch, C. Reller, H. Eckert, D. Hartmann, D. Taroata, K. Wiesner-Fleischer, A. Bulan, A. Lueken, G. Schmid, *Chem. Ing. Tech.* **2020**, *92*, 53–61.
[43] A. L. Rollet, J. P. Simonin, P. Turq, *Phys. Chem. Chem. Phys.* **2000**, *2*, 1029–1034.
[44] C. Tian, X. Y. Li, V. E. Nelson, P. Ou, D. Zhou, Y. Chen, J. Zhang, J. E. Huang, N. Wang, J. Yu, H. Liu, C. Liu, Y. Yang, T. Peng, Y. Zhao, B. H. Lee, S. Wang, E. Shirzadi, Z. Chen, R. K. Miao, D. Sinton, E. H. Sargent, *ACS Energy Lett.* **2023**, *8*, 4096–4103.
[45] E. J. Dufek, T. E. Lister, M. E. McIlwain, *J. Appl. Electrochem.* **2011**, *41*, 623–631.
[46] A. Löwe, C. Rieg, T. Hierlemann, N. Salas, D. Kopljar, N. Wagner, E. Klemm, *ChemElectroChem* **2019**, *6*, 4497–4506.
[47] E. J. Dufek, T. E. Lister, S. G. Stone, M. E. McIlwain, *J. Electrochem. Soc.* **2012**, *159*, F514–F517.
[48] H. Y. Kim, I. Choi, S. H. Ahn, S. J. Hwang, S. J. Yoo, J. Han, J. Kim, H. Park, J. H. Jang, S. K. Kim, *Int. J. Hydrogen Energy* **2014**, *39*, 16506–16512.
[49] T. Mizuno, K. Ohta, A. Sasaki, T. Akai, M. Hirano, A. Kawabe, *https://doi.org/10.1080/00908319508946098* **2010**, *17*, 503–508.
[50] S. M. A. Kriescher, K. Kugler, S. S. Hosseiny, Y. Gendel, M. Wessling, *Electrochem. Commun.* **2015**, *50*, 64–68.
[51] J. J. Kaczur, H. Yang, Z. Liu, S. D. Sajjad, R. I. Masel, *Front. Chem.* **2018**, *6*, 377597.
[52] B. Endrődi, E. Kecsenovity, A. Samu, F. Darvas, R. V. Jones, V. Török, A. Danyi, C. Janáky, *ACS Energy Lett.* **2019**, *4*, 1770–1777.

Manuscript received: January 15, 2024
Revised manuscript received: February 8, 2024
Version of record online: ■■, ■■

RESEARCH ARTICLE

Through systematic alteration of key components of acidic CO_2 electrolyzers, we were able to demonstrate production of multicarbon products at high current density and low cell voltage. Using a diaphragm in place of a membrane, altering the electrolyte composition and temperature, mixing the catholyte and anolyte, and reducing the distance between the electrodes, resulted in a stable, low-voltage device.

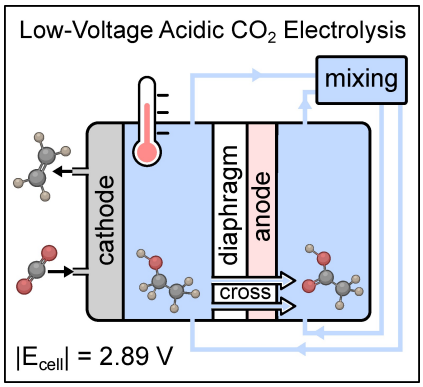

A. Perazio, M. W. Schreiber, C. E. Creissen, M. Fontecave**